Solar Wind and CMEs with the Space Weather Modeling Framework

Bart van der Holst, C. Downs, F. Fang, R. Oran, W. Manchester, G. Toth, T. Gombosi

Center for Space Environment Modeling
University of Michigan

http://csem.engin.umich.edu

Outline

- Default Solar Corona model at CCMC
- New: Two-temperature corona model with Alfvén waves
- New: Lower Corona model with EUV images
- New: Flux Emergence in Convection Zone model
- Future plans

Default Solar Corona Model at CCMC (O. Cohen et al.)

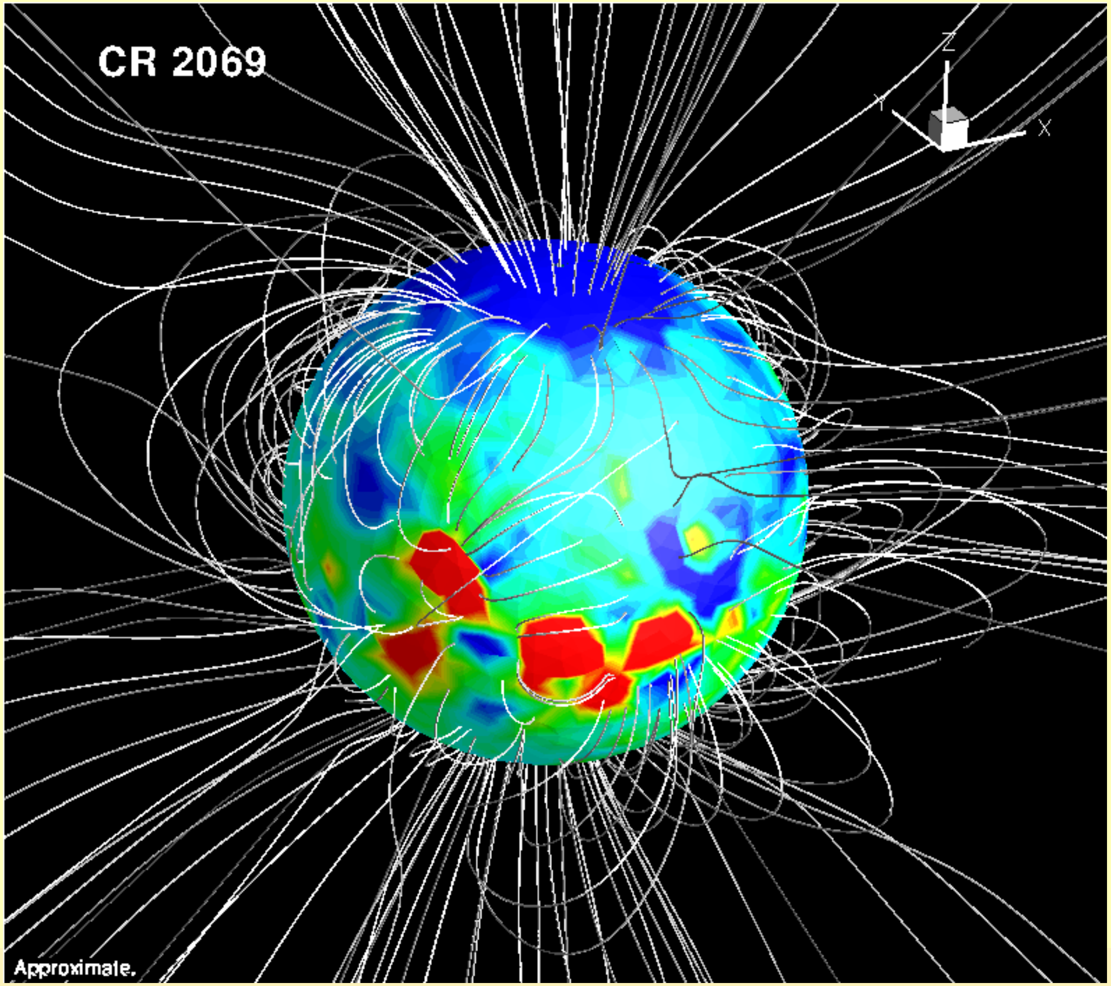

- Uses a spatially varying polytropic index γ to account for the coronal heating
- Uses the Wang-Sheeley-Arge model and Bernoulli integral along the field lines to determine γ
- Designed to reproduce the observations at 1AU

Quantitative Comparison with SOHO for the October 2003 Halloween Storm

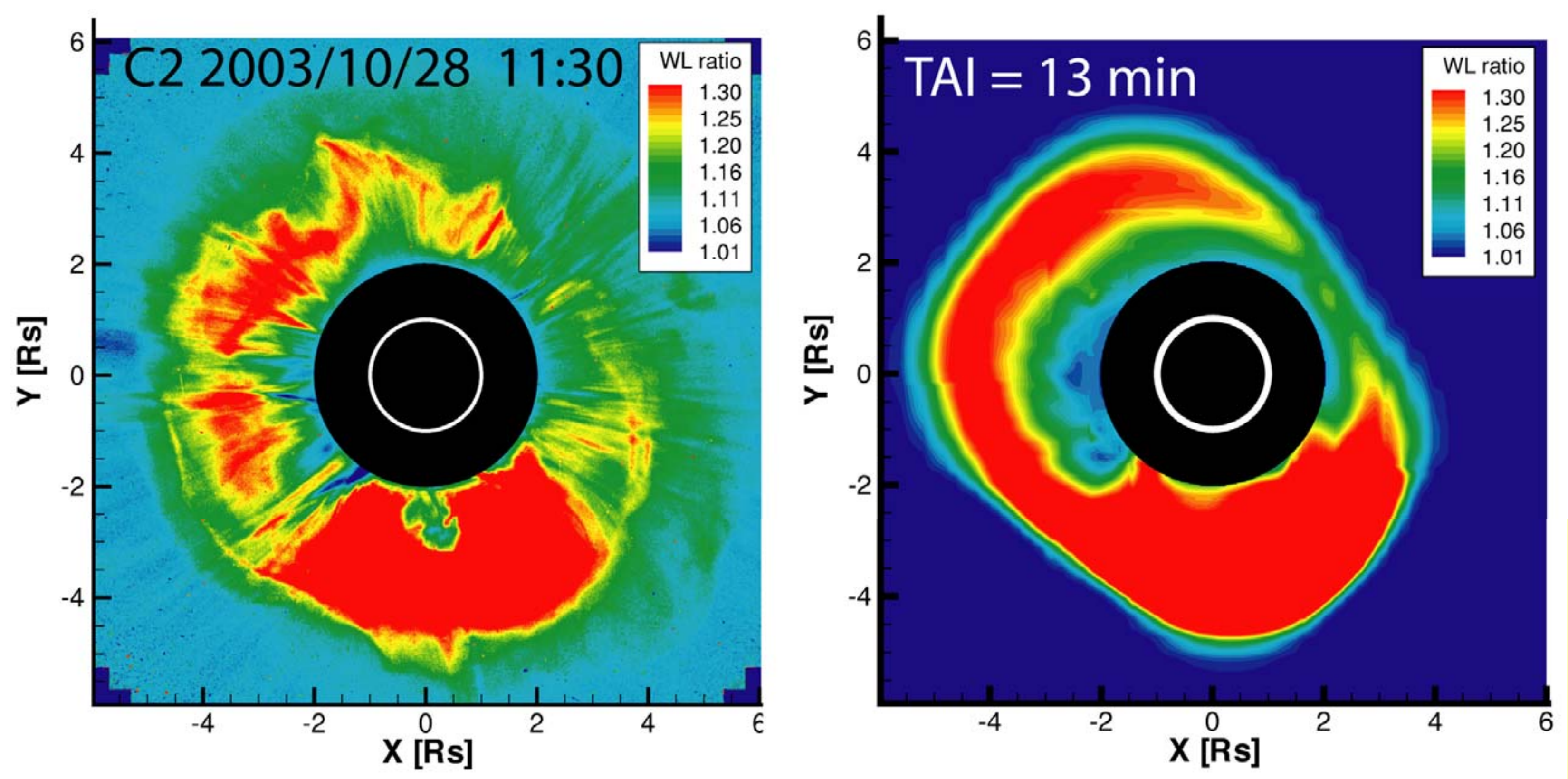

- Out of equilibrium flux rope superposed on a steady state MHD corona
- Total Mass, Observed =1.5×10^{16} gram Model = 2.2×10^{16} gram

Observed vs. Simulated Solar Wind and IMF near Earth (10º off)

Simulated CME arrives 4.8 hours early.

Solar wind speed is almost perfect!

Density is within range.

Magnetic field variation has right amplitude but sign and phase differ.

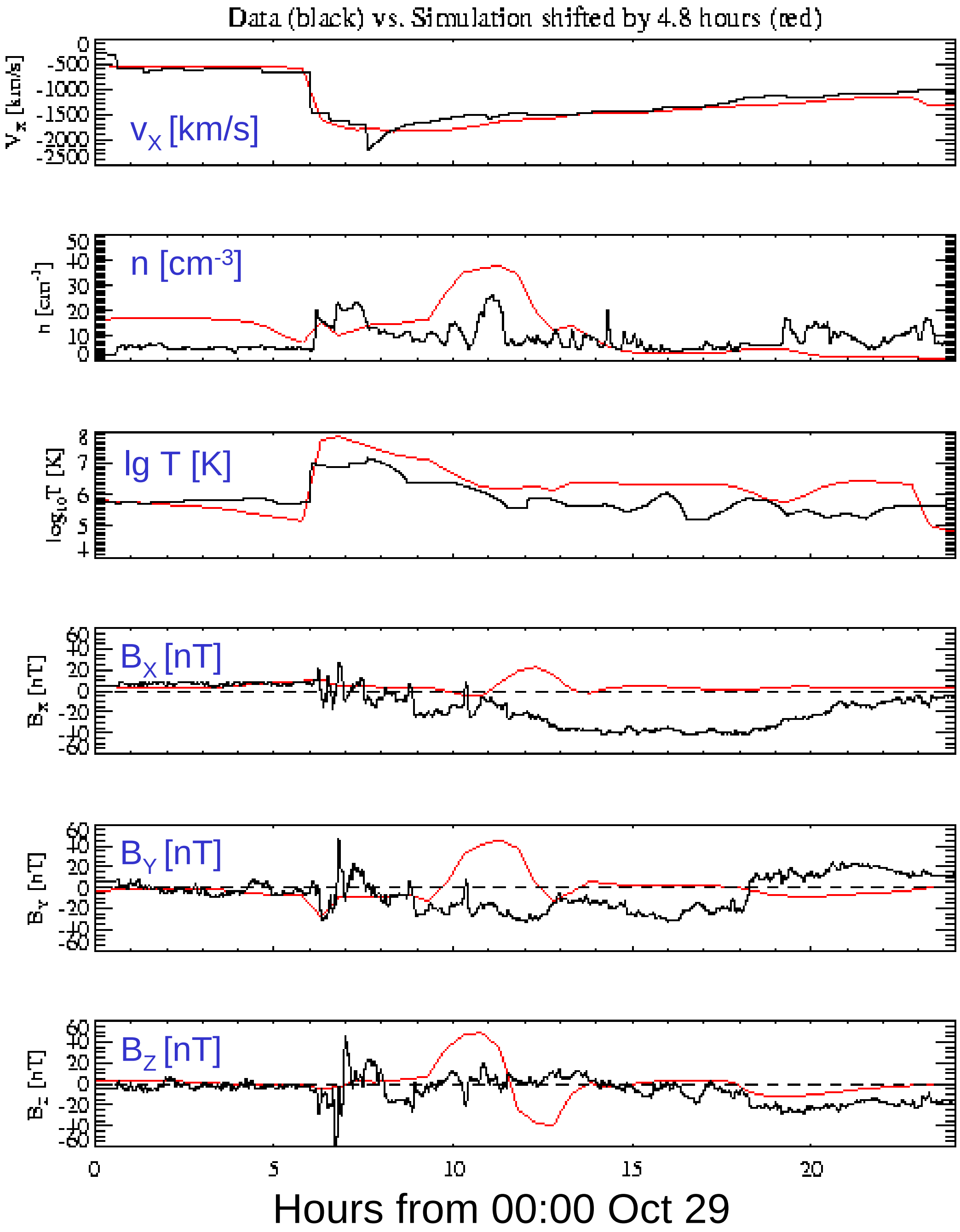

Room for improvement

- Midterm review of CCHM (Comprehensive Corona and Heliosphere Model):
  - Default Coronal model is based on a reduced, spatially varying adiabatic index for the heating and acceleration of the plasma.
  - In good agreement with the ambient solar wind observed at 1AU, but it is not self-consistent and distorts the physics, especially at CME shocks
- In addition: Default CME is not self-consistent, but a superposed flux rope model.

Improved Thermodynamics

- Use polytropic index γ =5/3
- Electrons are no longer heated by the ions beyond 1.5R_s, where electron-ion collisions is infrequent
- Ion heating (by Alfvén waves) is redistributed by ion heat conduction (35 times smaller than electron heat conduction)

$$\frac{\partial p_{\rm i}}{\partial t} + \nabla\cdot(p_{\rm i}\mathbf{u}) + (\gamma-1)p_{\rm i}\nabla\cdot\mathbf{u} = (\gamma-1)\left[Q_{\rm i} - \nabla\cdot\mathbf{q}_{\rm i} + \lambda_{\rm ei}(T_{\rm e}-T_{\rm i})\right],$$

$$\frac{\partial p_{\rm e}}{\partial t} + \nabla\cdot(p_{\rm e}\mathbf{u}) + (\gamma-1)p_{\rm e}\nabla\cdot\mathbf{u} = (\gamma-1)\left[\quad -\nabla\cdot\mathbf{q}_{\rm e} + \lambda_{\rm ei}(T_{\rm i}-T_{\rm e})\right],$$

$$\mathbf{q}_{\rm i} = -\kappa_{\rm i} T_{\rm i}^{5/2}\frac{\mathbf{BB}}{B^2}\cdot\nabla T_{\rm i}, \qquad \mathbf{q}_{\rm e} = -\kappa_{\rm e} T_{\rm e}^{5/2}\frac{\mathbf{BB}}{B^2}\cdot\nabla T_{\rm e}$$

- No collisionless heat conduction and additional electron heating yet

Code Verification

- **Verification of the new collisional heat conduction implementation**

$$\frac{\partial E_{\rm e}}{\partial t} = \cdots + \nabla \cdot \left(\kappa_{\rm e} T_{\rm e}^{5/2} \frac{\mathbf{BB}}{B^2} \cdot \nabla T_{\rm e} \right)$$

- **Diffusion of a Gaussian profile along the field lines**

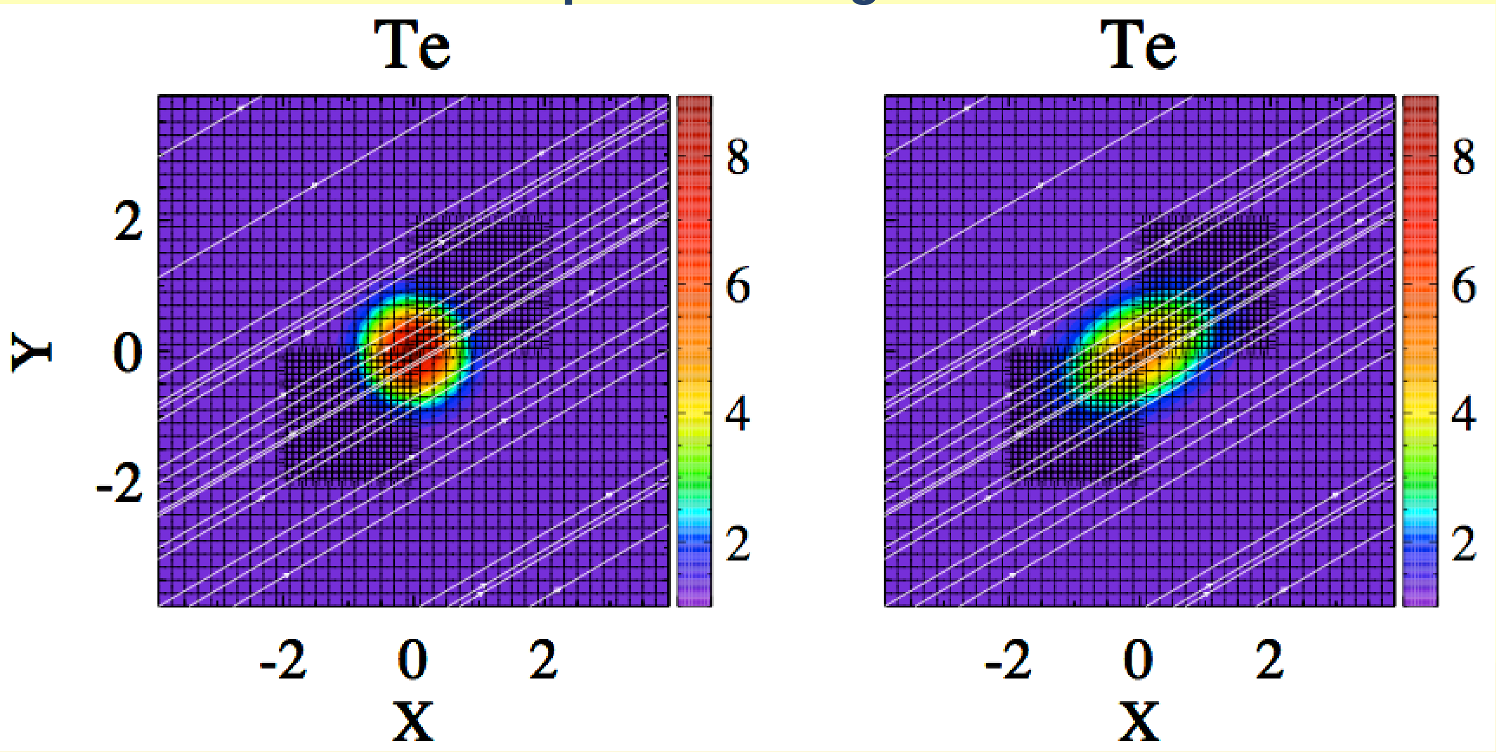

Code Verification

- **Verification of the new collisional heat conduction implementation**

$$\frac{\partial E_e}{\partial t} = \cdots + \nabla \cdot \left(\kappa_e T_e^{5/2} \frac{\mathbf{BB}}{B^2} \cdot \nabla T_e \right)$$

- **Diffusion of a Gaussian profile along the field lines**

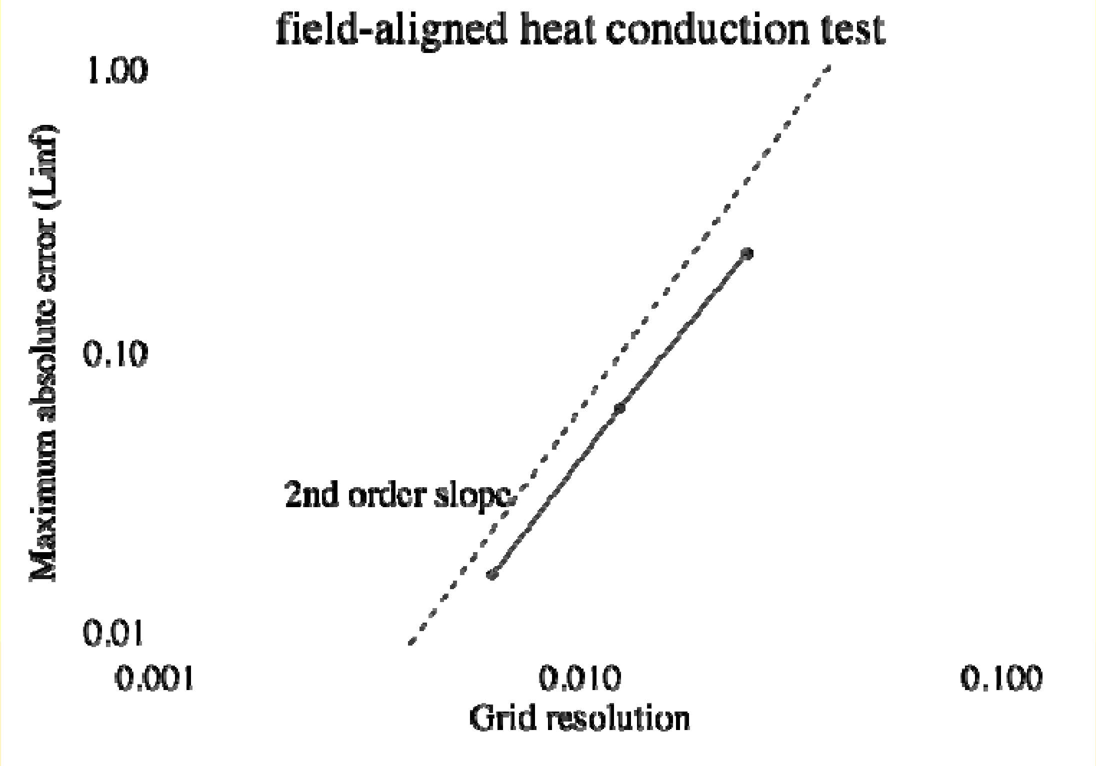

WKB Alfvén Waves

- **Hinode observations suggest that the Alfvén wave energy input is sufficient for heating and acceleration (e.g. de Pontieu et al. 2007).**
- **Wind acceleration: work done by wave pressure force**
- **Coronal heating: formulation of the Kolmogorov dissipation by Hollweg (1986)**

$$\frac{\partial E_{\rm w}^{+}}{\partial t} + \nabla\cdot\left[E_{\rm w}^{+}(\mathbf{u}+\mathbf{u}_{\rm A})\right] + p_{\rm w}^{+}\nabla\cdot\mathbf{u} = -Q^{+},$$

$$\frac{\partial E_{\rm w}^{-}}{\partial t} + \nabla\cdot\left[E_{\rm w}^{-}(\mathbf{u}-\mathbf{u}_{\rm A})\right] + p_{\rm w}^{-}\nabla\cdot\mathbf{u} = -Q^{-},$$

Ion heating $$Q_{\rm i} = Q^{+} + Q^{-} = \frac{{E_{\rm w}^{+}}^{3/2}}{L\sqrt{\rho}} + \frac{{E_{\rm w}^{-}}^{3/2}}{L\sqrt{\rho}}, \quad L = C/\sqrt{B},$$

- **Free parameter C in heating scale height L**

Model input

- **Magnetogram driven potential field extrapolation.**
- **Scale height of the heating and Alfvén wave dissipation.**
- **Specify Alfvén wave pressure at the solar base:**
  - Given solar wind expansion factor from PFSS model,
  - Given velocity at 1AU based on WSA model,
  - Impose energy conservation along the field lines to determine the Alfvén wave pressure at $1R_S$.

$$\frac{u_{\mathrm{WSA}}^2}{2} = \frac{\gamma}{\gamma-1}\frac{p_{\mathrm{i}}+p_{\mathrm{e}}}{\rho} - \frac{GM_{\odot}}{R_{\odot}} + R_{\odot}^2 \frac{|u_{\mathrm{A},r}|E_{\mathrm{w}}}{(\rho u r^2)_{1\mathrm{AU}} f_{\mathrm{expansion}}}$$

  - In-going Alfvén waves at $1R_S$ are absorbed.

Result for CR2077

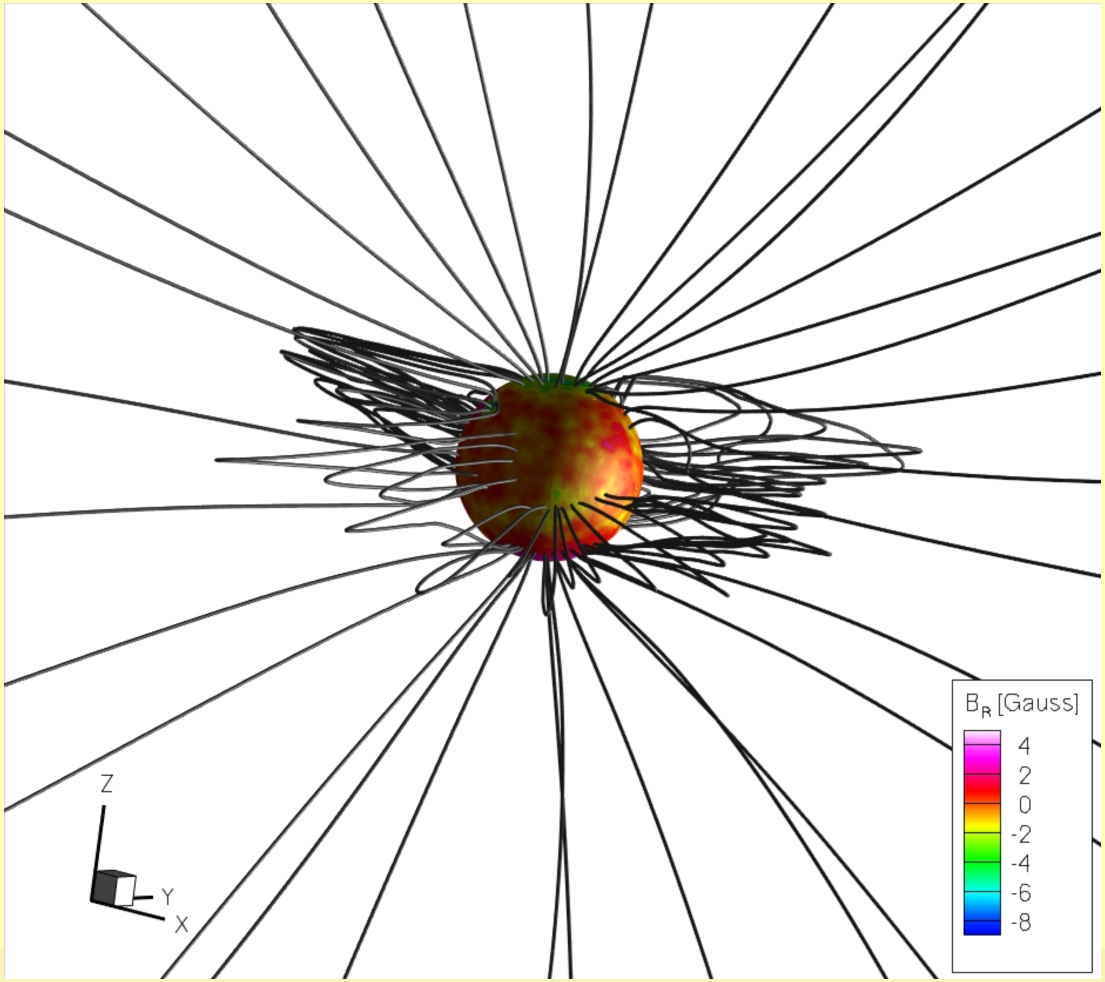

- **SOHO-MDI magnetogram CR2077**
- **Calculated on a 3D cartesian grid with AMR**
- **Predicted rms velocities of the Alfvén perturbations near the sun is of the order of 30km/s**

2T versus 1T model for CR2077

Radial velocity for 2 temperature model
Maximum is 785 km/s

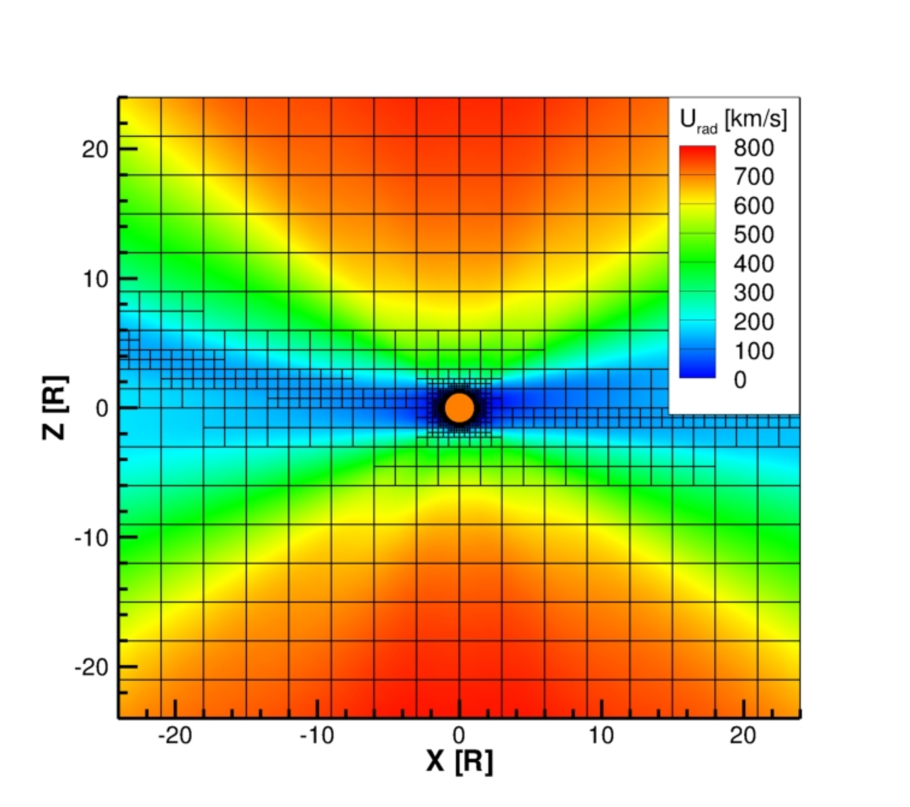

Radial velocity for 1 temperature model
Maximum is 714 km/s

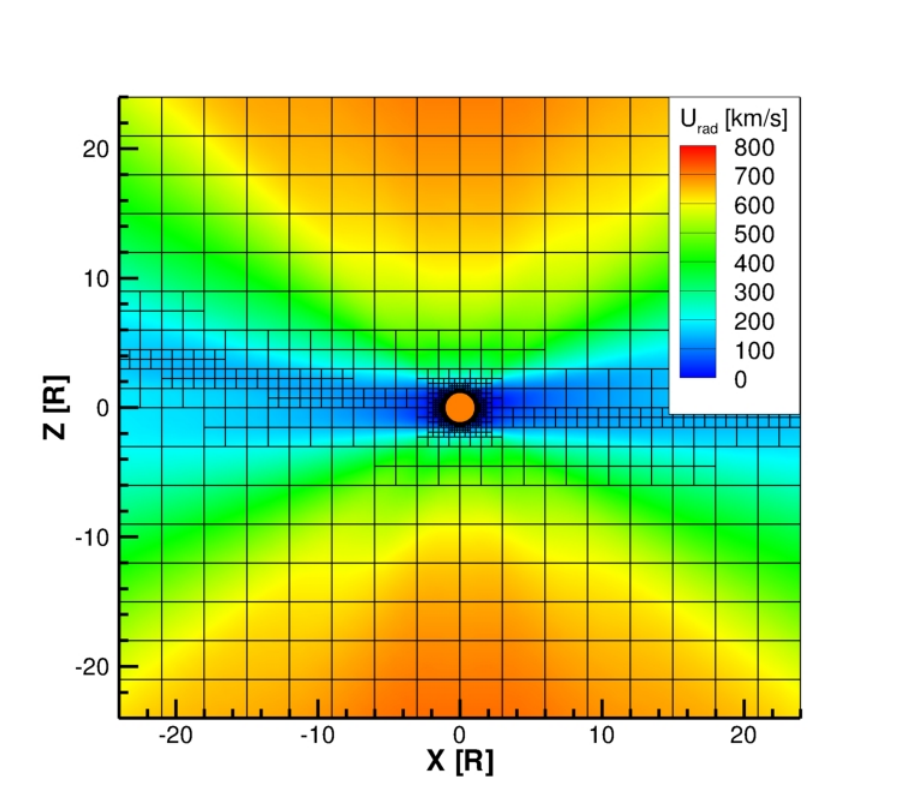

- **The black squares represent the AMR blocks of 4x4x4 cells**

2T versus 1T model for CR2077

Ion temperature

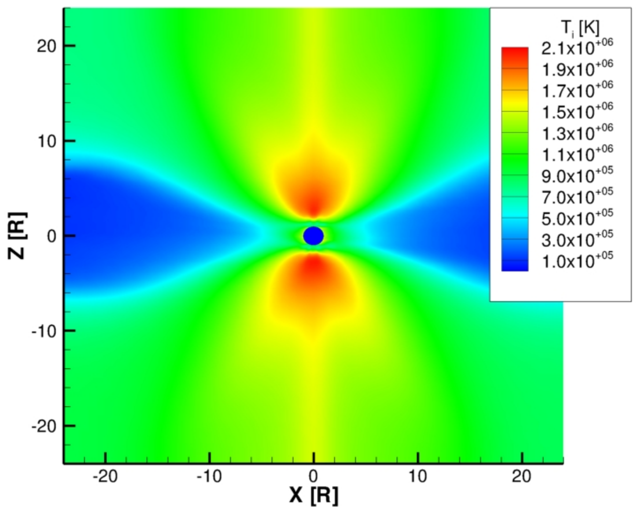

Electron temperature

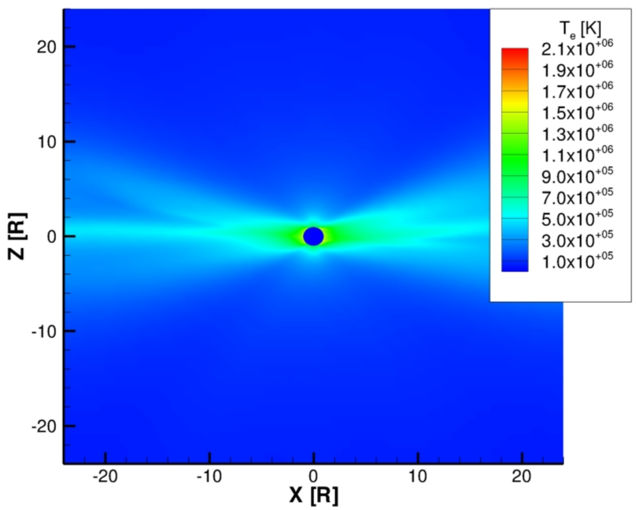

Temperature

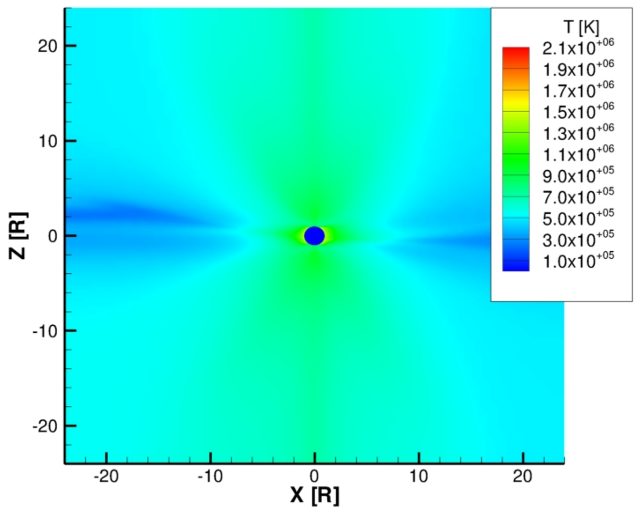

- **In the 2T model, the ions are preferentially heated in the coronal hole.**
- **In the 1T model: The strong spatial redistribution of the ion heating by the electron heat conduction is unphysical.**

Importance ion heat conduction

- Why using ion heat conduction if it is 35 times smaller than electron heat conduction ?

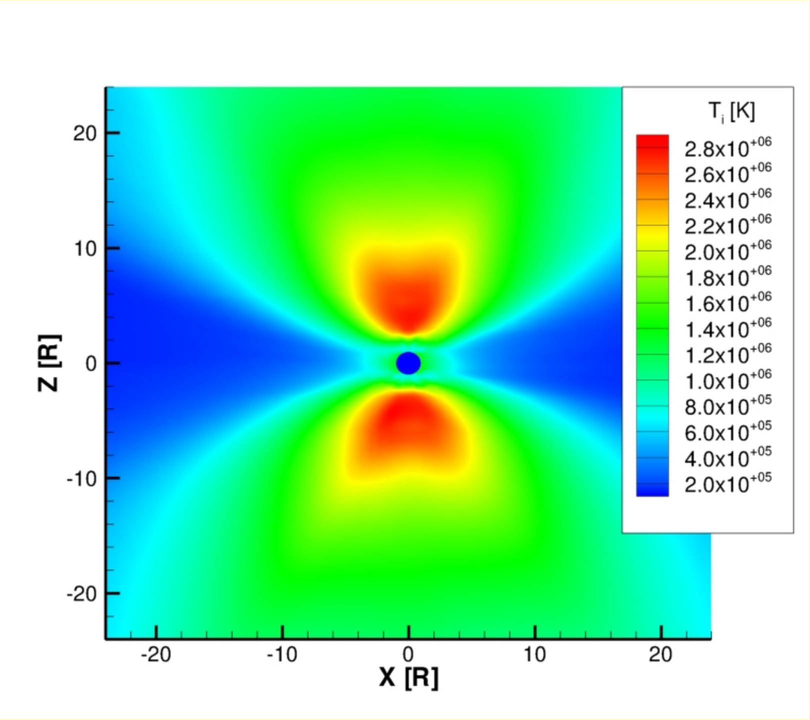

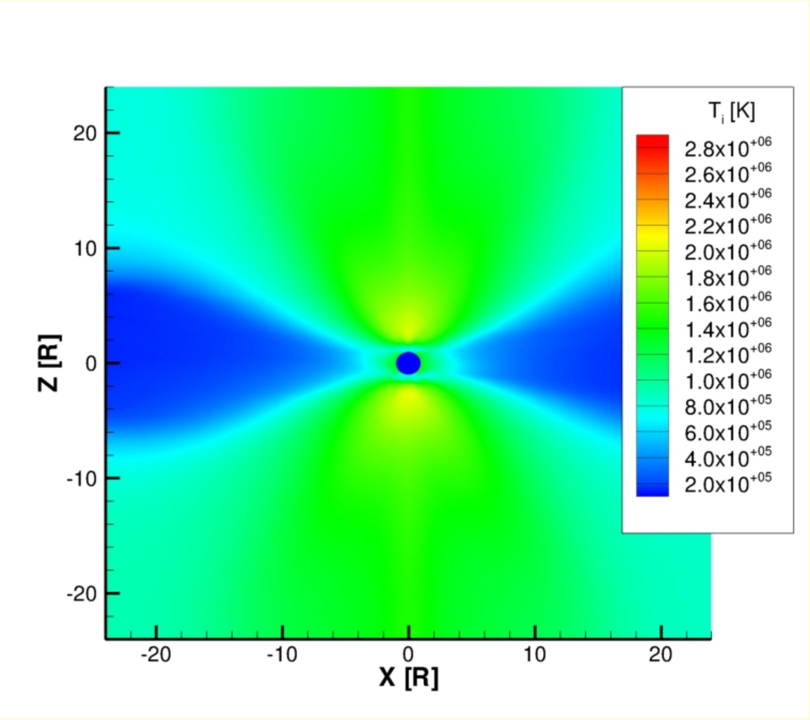

- 2T simulation without ion heat conduction
- Maximum ion temperature is 2.8MK

- 2T simulation with ion heat conduction
- Maximum ion temperature is 2.1MK

Lower Corona (C. Downs et al.)

- **Improved thermodynamics:**
  - One temperature model up to $1.5R_s$
  - Electron heat conduction with artificial broadening of the transition region (similar to Lionello et al. 2009)
  - Optically thin radiative losses
  - Exponential heating function, in active regions transition to heating proportional to magnetic field strength
- **Chromosphere boundary (T=20000K, $n_e=10^{12}$ cm^{-3})**
- **Ability to synthesize line-of-sight images in the EUV and X-ray regime**
- **Submitted to ApJ (C. Downs et al.)**

EUV and X-ray LOS images for CR1913

EIT 171Å EIT 195Å EIT 284Å SXT AlMg

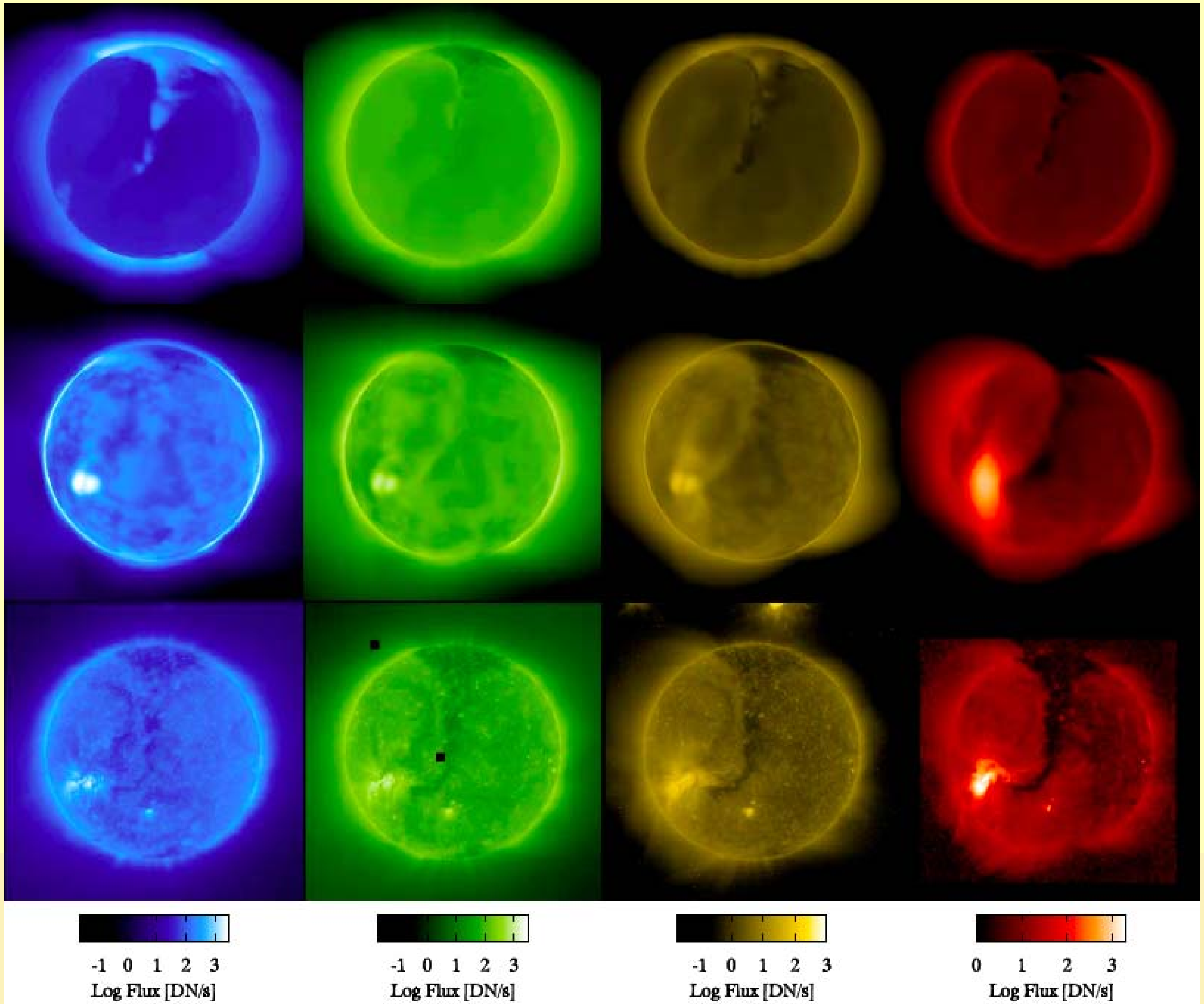

Old SC model synthesis

New LC model synthesis

Observation: Aug 27, 1997

Streamer structure for CR1913

PFSS model | Old SC model | New LC model

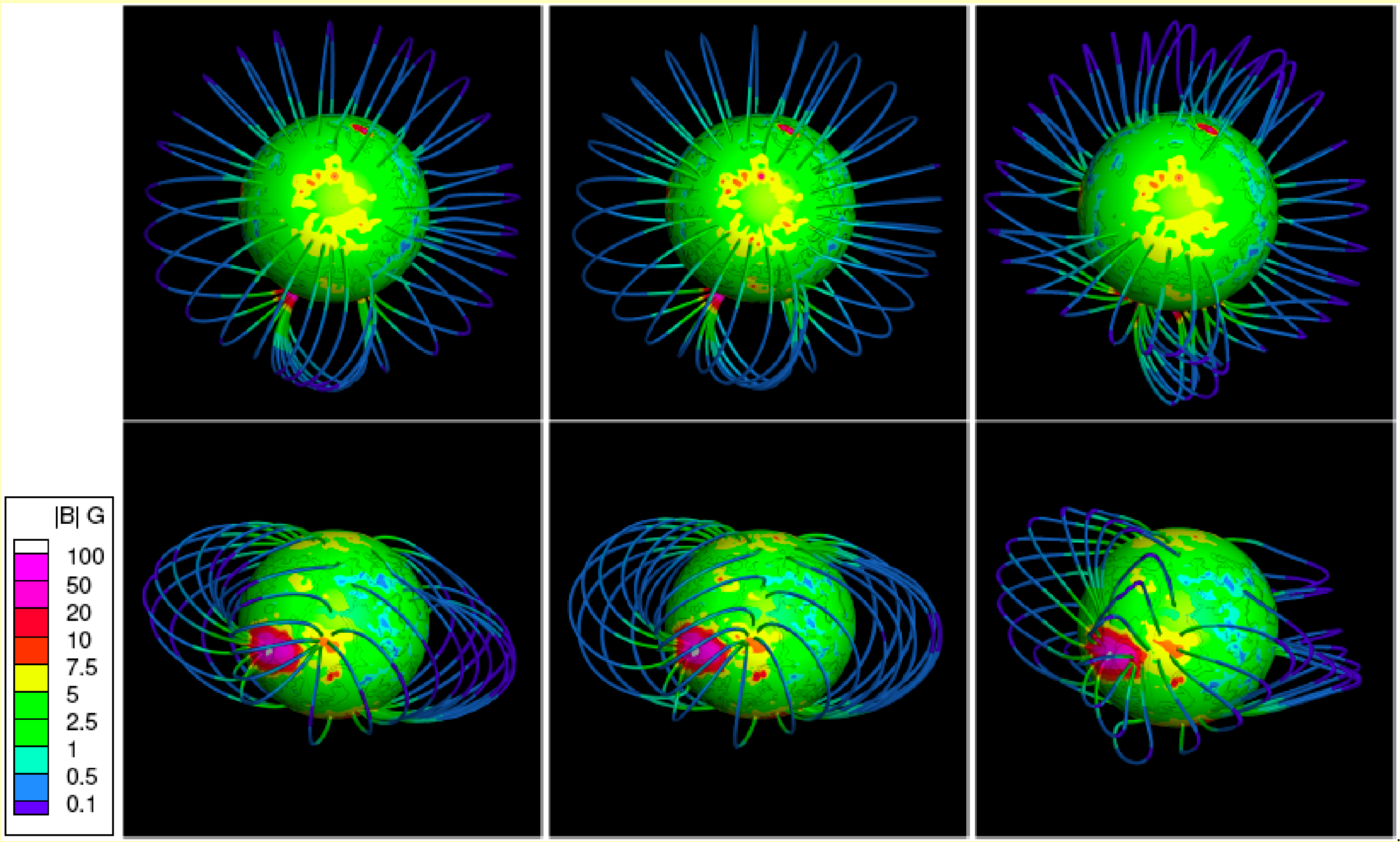

Top view

Earth Centered view

- **Closed field lines structures are stressed by heating near surface and subsequent redistribution via heat conduction**

SXT response for CR1913

3D topology of T=1.6MK

LOS synthesis of SXT AlMg response

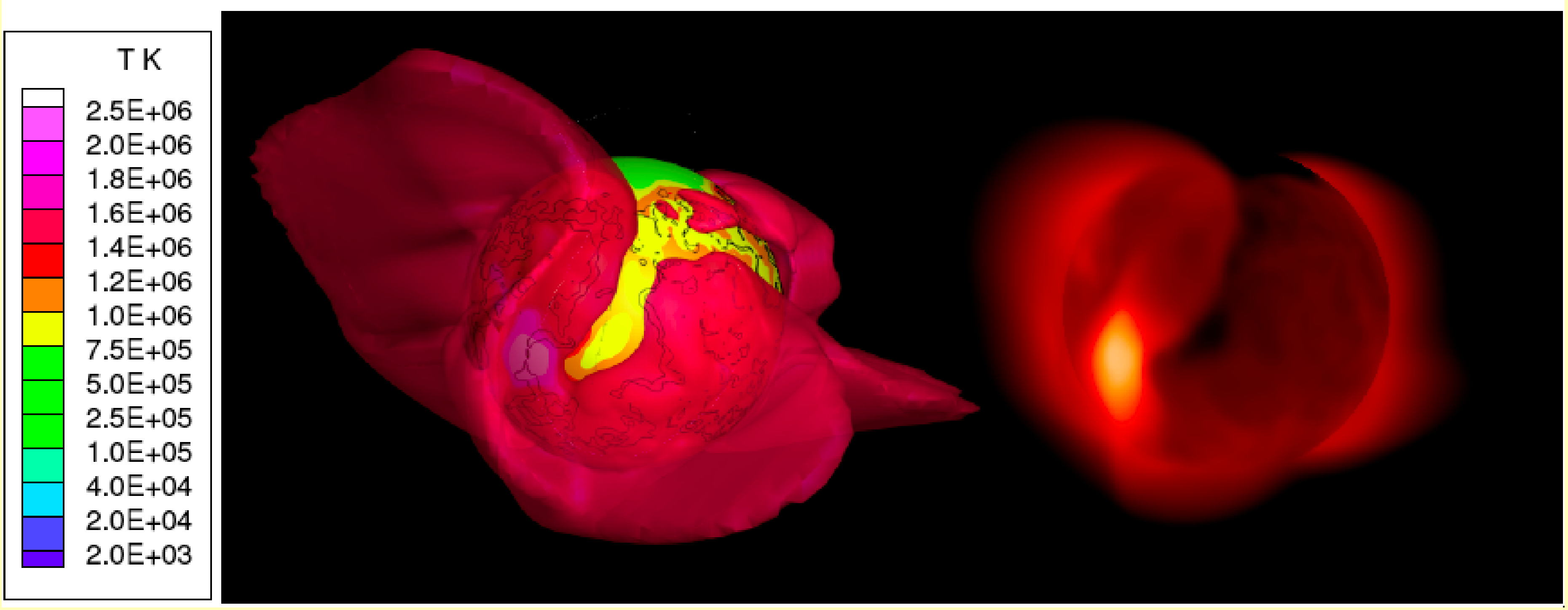

- **The hot, closed field line regions overlay the inversion lines on the surface and correspond to the x-ray emission.**

Convection Zone in BATSRUS (Fang et al.)

Atmosphere with coronal heating and radiative losses (Abbett, 2007)
OPAL EOS

Vertical velocity at photospheric level shown in gray scale

Magnetic field concentrated in the intergranular lanes

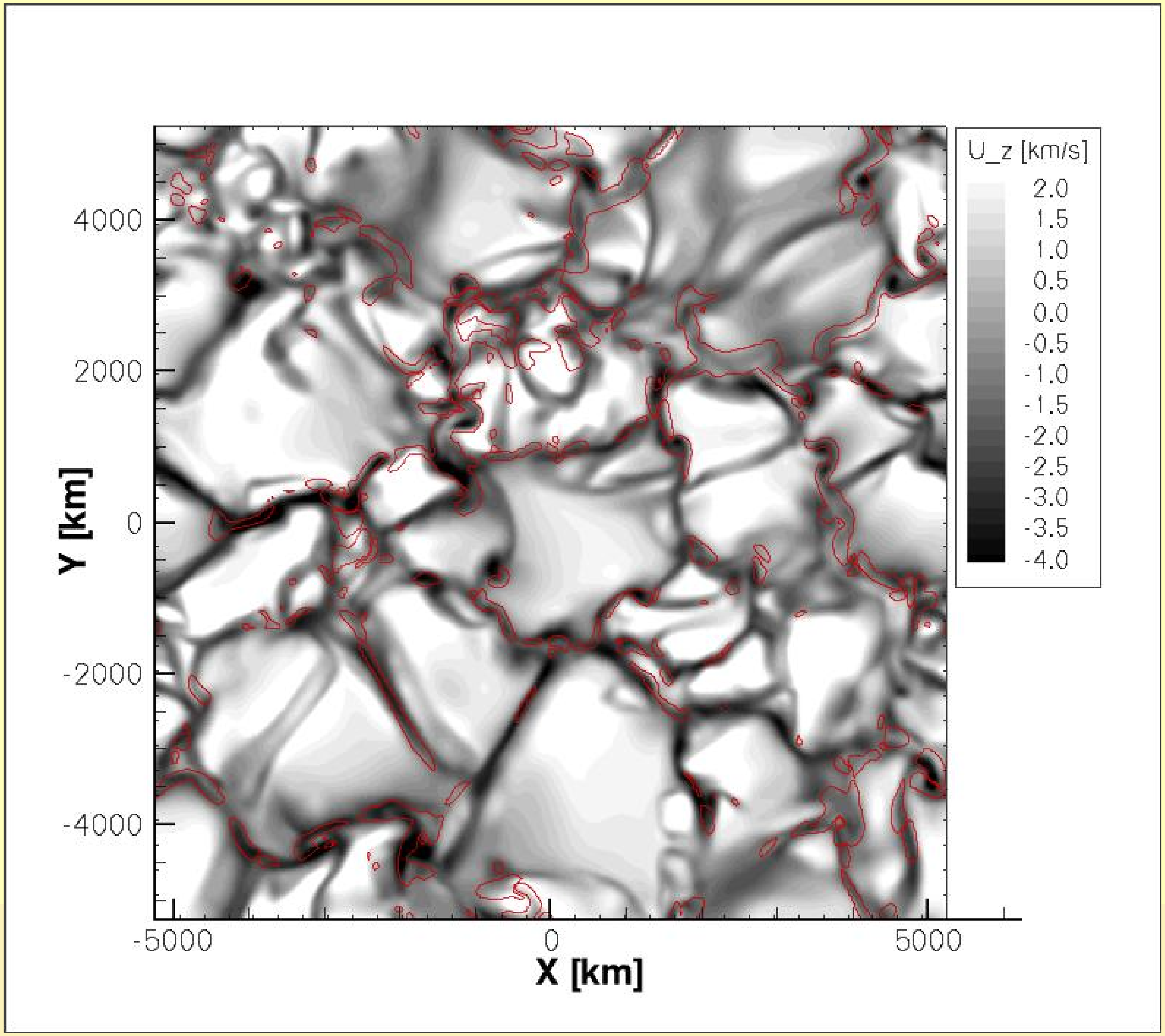

Flux Emergence In the Corona

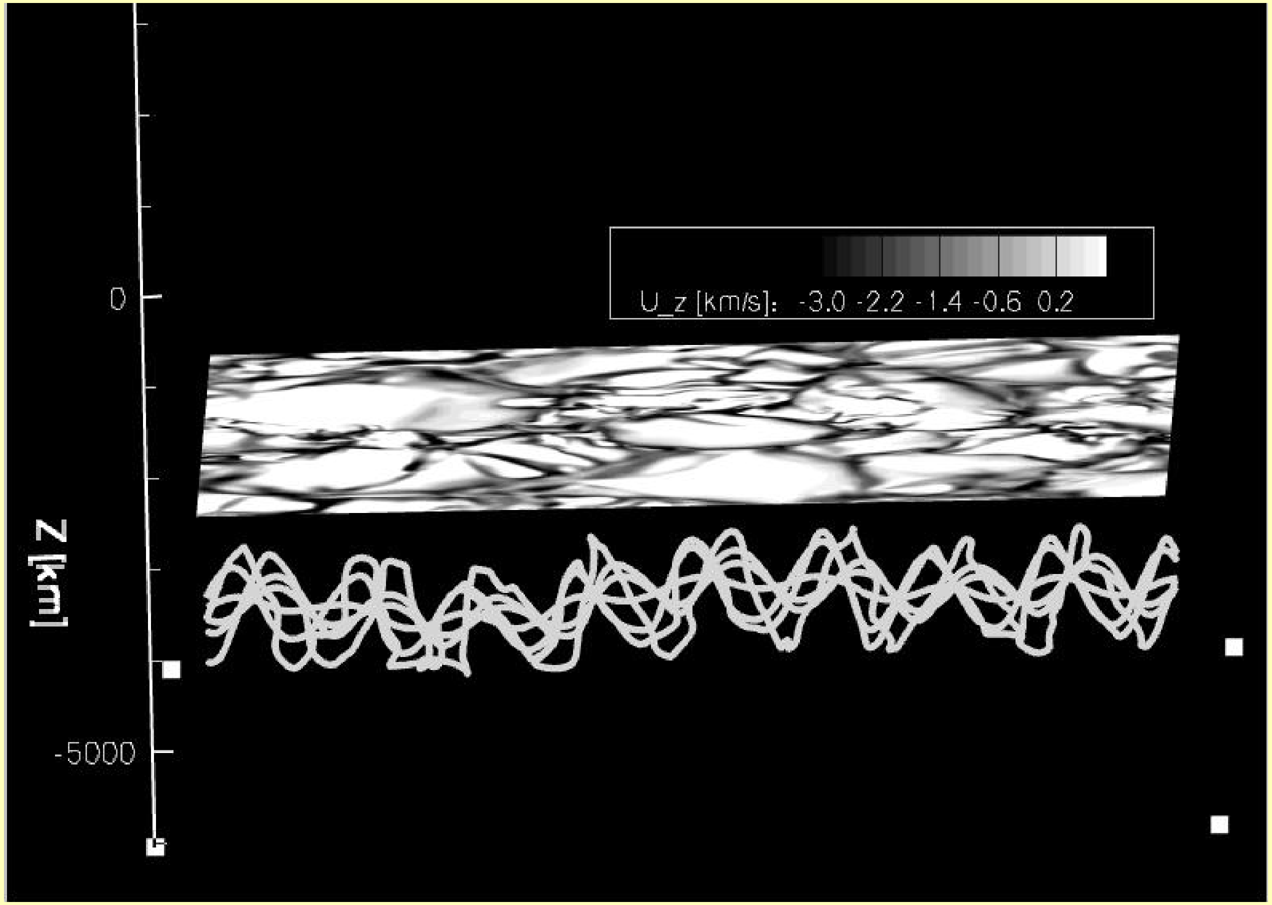

- Buoyant flux rope initially at 1500km below the photosphere
- 3D view at 2 minutes after initialization

Flux Emergence In the Corona

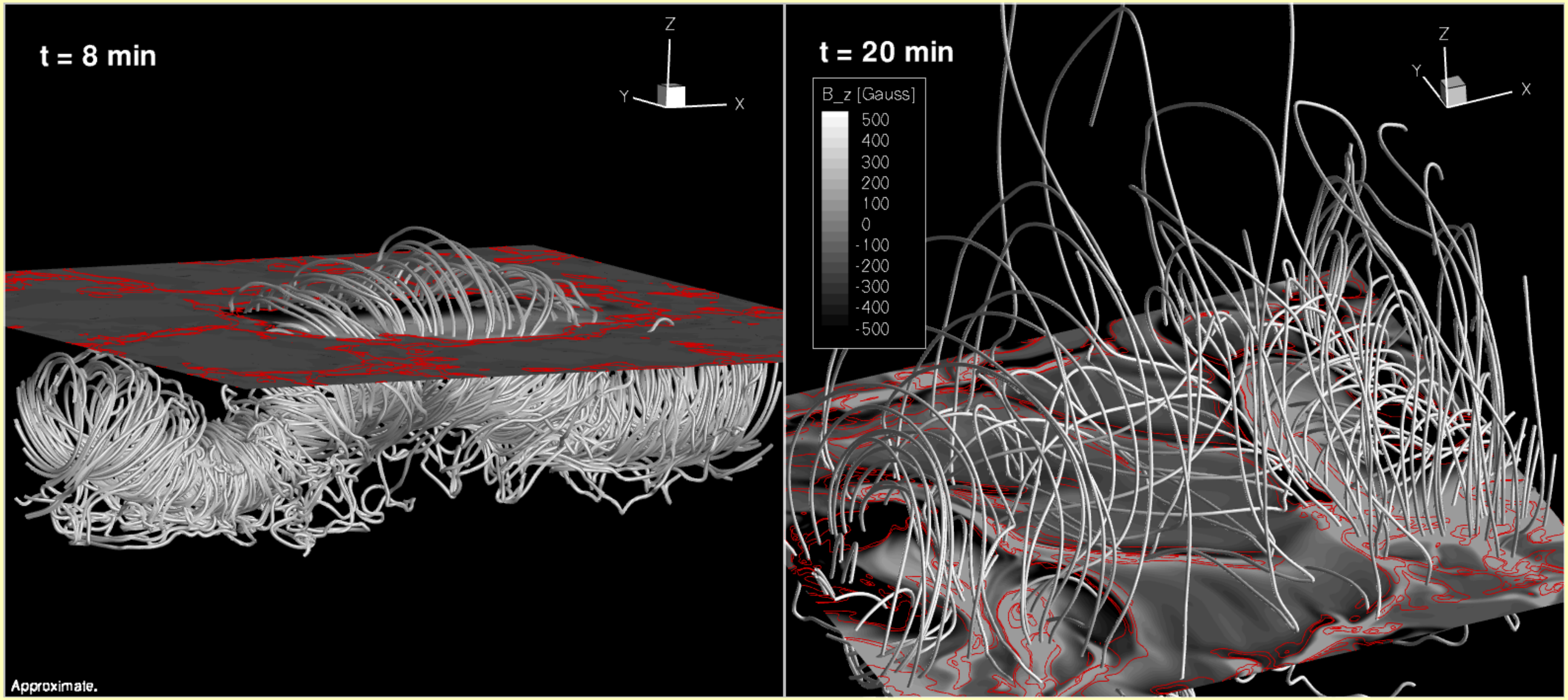

- Convective down flow tries to drag flux rope downwards, up flow helps the flux to emerge, thus segmentation of rope

Future plans

- Combine the two-temperature coronal model with the Alfvén wave turbulence model (see presentation Igor Sokolov)
- Use the newly developed radiation MHD package (gray and multigroup radiation diffusion) for the Convection Zone
- Couple the new Convection Zone, Lower Corona, Solar Corona, and Inner Heliosphere
- Do physically consistent CME eruptions into a physically consistent solar wind